

# **Lifetime Estimation of Cr<sub>2</sub>AlC MAX Phase Foam Based on Long-Term Oxidation and Fracture**

## **Mechanisms**

Wakako Araki<sup>a,\*</sup>, Asato Matsumoto<sup>a</sup>, Yoshio Arai<sup>a</sup>, Noriyasu Yamada<sup>a</sup>, Jürgen Malzbender<sup>b</sup>, and Jesus Gonzalez-Julian<sup>b,c</sup>

<sup>a</sup> Department of Mechanical Engineering, Saitama University, Japan

<sup>b</sup> Forschungszentrum Jülich GmbH, Institute of Energy and Climate Research, 52425 Jülich, Germany

<sup>c</sup> Department of Ceramics and Refractory Materials, Institute of Mineral Engineering, RWTH Aachen University, 52064 Aachen, Germany

\* Corresponding author. araki@mech.saitama-u.ac.jp (W. Araki); email: araki@mech.saitama-u.ac.jp

## ABSTRACT (250)

Oxidation kinetics and mechanical behaviour of  $\text{Cr}_2\text{AlC}$  foam with a porosity of 53 vol.% were investigated. Microstructures of  $\text{Cr}_2\text{AlC}$  foams oxidised in the temperature range 1173 to 1473 K for times between 0 and 100 h were examined. Uniaxial compression tests were performed at different temperatures in the range 298 to 1398 K to assess mechanical properties. The oxidation forms continuous with cohesive  $\text{Al}_2\text{O}_3$  layers on the  $\text{Cr}_2\text{AlC}$  matrix, beneath which porous  $\text{Cr}_7\text{C}_3$  is formed. The oxidation kinetics can be expressed by a parabolic law. An excessive oxidation takes place first in thin struts, where a breakage  $\text{Al}_2\text{O}_3$  layer occurs, followed by oxygen inflow and decomposition of inner material. At 298 K, non-oxidised  $\text{Cr}_2\text{AlC}$  foam fractures intergranularly. Slight oxidation improves compressive strength, as the  $\text{Al}_2\text{O}_3$  layer (2.5  $\mu\text{m}$  or thinner) can prevent cracks to propagate from inside outward. However, an excessive oxidation deteriorates any improvement due to the breakage of  $\text{Al}_2\text{O}_3$  layer in thin struts followed by the material decomposition. At 1273 K and 1398 K, non-oxidised porous  $\text{Cr}_2\text{AlC}$  fractures intergranularly, accompanied by a plastic deformation around small  $\text{Al}_2\text{O}_3$  particles segregated at grain boundaries. Oxidised  $\text{Cr}_2\text{AlC}$  foam with the  $\text{Al}_2\text{O}_3$  thickness of 2.5  $\mu\text{m}$  has a slightly higher brittle-to-plastic transition temperature ( $\sim 1273$  K) than dense  $\text{Cr}_2\text{AlC}$ . A thicker  $\text{Al}_2\text{O}_3$  layer ( $\sim 5$   $\mu\text{m}$ ) is required to reinforce the material due to inferior mechanical properties of  $\text{Cr}_2\text{AlC}$  at high temperatures. On the basis of the elucidated oxidation and fracture mechanisms, a safety criterion for high-temperature applications is suggested.

*Keywords:* MAX phases;  $\text{Cr}_2\text{AlC}$ ; Mechanical properties; Porous materials; Oxidation; Lifetime

## 1. Introduction

MAX phases are layered materials with a general formula of  $M_{n+1}AX_n$ , where M is an early transition metal, A is an A-group element of the periodic table, X corresponds to C and/or N, and  $n$  is typically 1, 2, or 3 [1]. They have attracted a strong interest because of their unique combination of properties, bridging the gap between metals and ceramics [2]. Whilst more than 80 different MAX phases have been discovered to date, MAX phases that contain aluminium as “A” element are of particular interest for high temperature applications, since these Al-based MAX phases form under oxidizing atmosphere at high temperature, typically  $> 1273$  K, an external, cohesive and dense  $\alpha$ - $Al_2O_3$  layer that protects the material against further oxidation [3][4].

Among all the Al-based MAX phases,  $Ti_2AlC$ ,  $Ti_3AlC_2$ , and  $Cr_2AlC$  appear to possess the best oxidation and corrosion resistances [3], and so these MAX phases are excellent candidates to be operated at high temperature under aggressive environments due to the above mentioned response and the combination of other characteristic features of MAX phases, such as lightweight, high elastic modulus, thermal and electrical conductivity, good machinability with excellent thermal shock resistance and damage tolerance [5][6][7][8].

Whilst the excellent properties of MAX phases have triggered the development of various structures such as thin films and composites [9][10], porous MAX phases have been investigated to a minor extent despite their high potentials for various applications such as catalyst supports and heat exchangers. In fact, a number of main drawbacks of reticular ceramic structures, i.e., high brittleness, hard machining, complex joining with metals, and high coefficient of thermal expansion mismatch, could be overcome by using MAX phase foams. Most of the studies on MAX phase foams published to date are mainly focused on processing routes [11][12][13][14][15]. Different routes lead to tailor diverse final microstructures, such as porosity, pore size, and thickness of struts. Recently,  $Cr_2AlC$  foams have been produced by a sacrificial template and replica method [16][17].

The oxidation kinetics of  $\text{Cr}_2\text{AlC}$  was also investigated in a number of studies, and its excellent oxidation resistance was demonstrated [3][18][19][20][21]. The oxidation starts at a temperature of  $\sim 1073\text{K}$  and leads to a dense and cohesive  $\text{Al}_2\text{O}_3$  layer on the outer surface of  $\text{Cr}_2\text{AlC}$  owing to the outward diffusion of Al, beneath which porous  $\text{Cr}_7\text{C}_3$  is formed. Effects of various factors such as cyclic oxidation and grain size on the oxidation were reported [5][22][23]. Also, a crack self-healing effect in  $\text{Cr}_2\text{AlC}$  due to the oxide scale formation was confirmed [24][25]. Most of the studies suggested that the oxidation kinetics of  $\text{Cr}_2\text{AlC}$  could be parabolic, whereas it has also been claimed that the oxidation kinetics of  $\text{Cr}_2\text{AlC}$  could be more complex, not expressed by a simple parabolic or cubic model [3]. The oxidation of porous  $\text{Cr}_2\text{AlC}$  has been also reported, which also confirmed remarkable formations of  $\text{Al}_2\text{O}_3$  and  $\text{Cr}_7\text{C}_3$  above  $1073\text{ K}$ . It should be noted that  $\text{Cr}_2\text{AlC}$  is the only Al-based MAX phase which forms a carbide layer ( $\text{Cr}_7\text{C}_3$ ) beneath  $\text{Al}_2\text{O}_3$  layer after oxidation; however, the formation of  $\text{Cr}_7\text{C}_3$  is quite problematic, because it could be easily oxidised in case of a breakage of  $\text{Al}_2\text{O}_3$  layer, which will be catastrophic [3].

Compared to those studies on processing and oxidation of  $\text{Cr}_2\text{AlC}$ , the number of studies in literature on the mechanical properties is quite limited [24-30]. Mechanical properties of  $\text{Cr}_2\text{AlC}$  such as Young's modulus, flexural strength, and fracture toughness were studied mostly at room temperature [29-31]. Young's modulus and compressive strength at room temperature are found to be  $288\text{ GPa}$  and  $1159\text{ MPa}$  [28], respectively, which are comparable to other Al-based MAX phases such as  $\text{Ti}_3\text{AlC}_2$  and  $\text{Nb}_2\text{AlC}$  [7]. Effects of various factors, such as impurity [30] and thermal shock [31], on the mechanical properties were investigated, whilst elastic properties determined by ab-initio molecular dynamics simulation were compared to the experimental values [29]. The temperature dependence of mechanical behaviour was also investigated on the basis of four-point bending tests, which revealed that the brittle-to-plastic transition occurs between  $1073\text{ K}$  and  $1273\text{ K}$  [32], close to that of the other Al-containing MAX phases, i.e.,  $\text{Ti}_2\text{AlC}$  [33] and  $\text{Ti}_3\text{AlC}_2$  [34].

The number of studies on mechanical properties of  $\text{Cr}_2\text{AlC}$  foam is even more limited. Recently, the compressive strength of  $\text{Cr}_2\text{AlC}$  foam was investigated in a uniaxial compression test at room temperature, which demonstrated that a pre-oxidation of  $\text{Cr}_2\text{AlC}$  foam at 1473 K for 1 h can significantly improve the compressive strength [16]. The effect of porosity on creep deformation behaviour of  $\text{Cr}_2\text{AlC}$  foam was investigated at elevated temperatures [26], which also revealed that the pre-oxidation can improve the creep resistance of  $\text{Cr}_2\text{AlC}$  foam by a few orders of magnitude. Both of the studies on the mechanical responses of  $\text{Cr}_2\text{AlC}$  foam have attributed the observed reinforcements to the oxide scales formed on the surface by the pre-oxidation; however, the oxidation kinetics and reinforcement mechanisms of  $\text{Cr}_2\text{AlC}$  foam are not well understood yet.

The aim of the current work is to investigate the oxidation mechanism and mechanical behaviour of  $\text{Cr}_2\text{AlC}$  foam.  $\text{Cr}_2\text{AlC}$  foam containing 53 vol.% porosity was oxidised at temperatures between 1173 K and 1473 K for times between 0 and 100 h, and the respective microstructure was examined. Uniaxial compression tests were performed at 298 K, 1273 K, and 1398 K using  $\text{Cr}_2\text{AlC}$  foams pre-oxidised at 1473 K for times between 0 and 50 h to examine mechanical properties, i.e., compressive strength and Young's modulus. On the basis of the results, the oxidation and fracture mechanisms of  $\text{Cr}_2\text{AlC}$  are elucidated, and a safety criterion for application is suggested.

## **2. Experimental**

Processing of porous  $\text{Cr}_2\text{AlC}$  was carried out in two consecutive steps. First,  $\text{Cr}_2\text{AlC}$  powder was synthesized from its elemental constituents by liquid/solid state reaction, followed by a second step to consolidate porous samples at high temperature as reported with more details in [26][16]. Briefly, Cr, Al, and C powders (all from Alfa Aesar, Germany) were mixed in a molar ratio of 2:1.1:1, respectively, and uniaxially pressed at 100 MPa. Pellets were heated at 1673 K in argon atmosphere for 3 h to synthesize the  $\text{Cr}_2\text{AlC}$  phase. Then,  $\text{Cr}_2\text{AlC}$  samples were ground and milled to obtain the final powder with a unimodal particle size distribution and a mean particle size of 9  $\mu\text{m}$ . Porous samples were produced by a sacrificial

template method, using ammonium hydrogen bicarbonate ( $\text{NH}_4\text{HCO}_3$ ) as temporary space holder material.  $\text{Cr}_2\text{AlC}$  powder was mixed with 60 vol.% of  $\text{NH}_4\text{HCO}_3$ , followed by cold uniaxial pressing to obtain pellets of 13 mm diameter and 10 mm height. The space holders were burned-out at low temperature (353 K) in air, and the porous structures were consolidated at 1523 K for 5 h in argon atmosphere. The consolidated porous samples possessed a final porosity of 53 vol.% with pore sizes between 180 and 250  $\mu\text{m}$ . The microstructure of the prepared sample is reported in detail in a previous study [18].

The prepared porous  $\text{Cr}_2\text{AlC}$  was cut into rectangular bar samples with dimensions of approximately  $2.5 \times 2.5 \times 6 \text{ mm}^3$  using a diamond wheel saw. The bar samples were annealed at 1273 to 1473 K for 1 to 100 h in ambient air using an electric furnace. (Note that the oxidation at 1173 K and lower was too slow for the present evaluation.) The cross-section of the annealed samples was polished with abrasive papers (#2000) and investigated using a scanning electron microscope (SEM) and energy dispersion X-ray analysis (EDX) (TM3030, Hitachi High-Technologies) to examine the microstructure.

Then, the mechanical behaviours of porous  $\text{Cr}_2\text{AlC}$  annealed at 1473 K for different times were examined via uniaxial compression tests using a universal testing machine (AGS-X, Shimadzu) with an infrared furnace (IR-TP1-2, Yonekura). The testing temperatures were 298, 1273, and 1398 K with heating rates of 25–100 K/min. Each individual specimen was heated to the test temperature under a small pre-load of 0–5 MPa, followed by a holding period (20 min), and then the compressive stress was applied to the sample with the loading rate of 0.5 MPa/s. The specimen was rapidly cooled down after the test. All the test process (from the start of heating to the end of cooling) was finished within 30 min to avoid further oxidation for subsequent observation of fracture surfaces. The strain was measured using strain gauges (FLA, Tokyo Sokki) at room temperature, whilst only the displacement of the loading head was recorded at high temperatures. The obtained mechanical properties, i.e., compressive strength at each temperature and Young's modulus only at 298 K, are discussed especially their relationship to variations in microstructure.

### 3. Results

### 3.1 Microstructure of oxidised porous $\text{Cr}_2\text{AlC}$

Figure 1 shows the SEM images of polished cross-sections of porous  $\text{Cr}_2\text{AlC}$  specimens annealed at 1473 K for 3 h, 10 h, and 50 h (general views in (a)–(c) and at higher magnifications in (d)–(f)), respectively, where the material compositions shown here are assigned by the additional EDX analysis. The formation and growth of  $\text{Al}_2\text{O}_3$  with porous  $\text{Cr}_7\text{C}_3$  layers beneath are clearly observable (Fig. 1(a) and (d)), as similarly reported for dense  $\text{Cr}_2\text{AlC}$  in the previous studies [3][19]. The thickness of  $\text{Al}_2\text{O}_3$  layer on the surface increases with annealing time, whilst the  $\text{Cr}_7\text{C}_3$  layer beneath the  $\text{Al}_2\text{O}_3$  grows thicker with a higher apparent rate and simultaneously becomes very porous (Fig. 1(b)). Accompanied by the formation of  $\text{Al}_2\text{O}_3$  and  $\text{Cr}_7\text{C}_3$ , the remaining volume of porous  $\text{Cr}_2\text{AlC}$  matrix decreases with the annealing time. In addition to  $\text{Cr}_7\text{C}_3$ ,  $\text{Cr}_2\text{O}_3$  starts to appear in the sample annealed for 10 h (Fig. 1(b) and (e)), which grows then further with the annealing time up to 50 h, whilst some  $\text{Al}_2\text{O}_3$  domains start to appear not only on the surface but also inside of the samples (Fig. 1(c)). In addition, the outer surface of  $\text{Al}_2\text{O}_3$  becomes slightly porous after longer annealing (Fig. 1(f)), as similarly reported for dense  $\text{Cr}_2\text{AlC}$  [24]. The sample annealed for 50 h at 1473 K consists predominantly of  $\text{Al}_2\text{O}_3$ ,  $\text{Cr}_7\text{C}_3$ , and  $\text{Cr}_2\text{O}_3$ , whilst there is only a small amount of remaining  $\text{Cr}_2\text{AlC}$  matrix.

Figure 2 summarises the thickness of  $\text{Al}_2\text{O}_3$  layer  $\Delta h$  formed on the porous  $\text{Cr}_2\text{AlC}$  annealed at different temperatures in the range 1273 K to 1473 K for times between 0 and 100 h, where the  $\text{Al}_2\text{O}_3$  thickness was determined on the basis of three SEM images with five different measuring points each. The  $\text{Al}_2\text{O}_3$  layer becomes thicker for the samples annealed at higher temperature for longer annealing times, which agrees with the observations for dense  $\text{Cr}_2\text{AlC}$  [36]. The specimens with the same  $\text{Al}_2\text{O}_3$  thickness have similar microstructures regardless of annealing condition. (It should be noted that the thickness of  $\text{Cr}_7\text{C}_3$  layer was too varied all over the specimen to determine its average thickness, unlike  $\text{Al}_2\text{O}_3$ .)

### 3.2 Mechanical properties of oxidised porous $\text{Cr}_2\text{AlC}$

Figure 3(a) presents the stress vs strain relationships of porous  $\text{Cr}_2\text{AlC}$  pre-annealed at 1473 K for different times, obtained via uniaxial compression tests at 298 K. The relationships are mostly linear, and

all the specimens fractured in a brittle manner. Figure 3(b) and 3(c) present the stress vs displacement relationships obtained via the uniaxial tests at 1273 K and 1398 K, respectively. Some specimens tested at 1273 K, especially the ones annealed for short times at 1473 K, and all the specimens tested at 1398 K revealed a large plastic deformation before fracture or collapse. During the plastic deformation, the stress vs displacement curves displayed a number of small spikes, especially for the samples annealed for shorter times or tested at higher temperature (1398 K).

Figure 4 summarises the compressive strength of porous  $\text{Cr}_2\text{AlC}$  annealed at 1473 K for different hours in relation to  $\text{Al}_2\text{O}_3$  thickness, where the compressive strength was evaluated using the maximum stress before large plastic deformations occurred. (Note that the thickness of  $\text{Al}_2\text{O}_3$  layer formed on the specimens tested at high temperatures was re-evaluated using specimens separately annealed under the same conditions in order to take into account a growth of  $\text{Al}_2\text{O}_3$  layer during the compression test, although its growth was quite small). The compressive strength at 298 K shows a significant increase from 76 MPa to 153 MPa when the  $\text{Al}_2\text{O}_3$  thickness increased from 0 to  $\sim 2.5 \mu\text{m}$ , followed by a gradual decrease to 50 MPa with increase of the  $\text{Al}_2\text{O}_3$  thickness to  $7.6 \mu\text{m}$ . At 1273 K, the compressive strength of porous  $\text{Cr}_2\text{AlC}$  (without pre-oxidation) is considerably lower than the strength at 298 K, and the  $\text{Al}_2\text{O}_3$  layer of  $3 \mu\text{m}$  does not yet reinforce the porous  $\text{Cr}_2\text{AlC}$  unlike at 298 K. However, the strength shows a noticeable increase reaching a maximum of 138 MPa for an  $\text{Al}_2\text{O}_3$  thickness of  $4.9 \mu\text{m}$ , followed by a slight decrease to 110 MPa with increase of the  $\text{Al}_2\text{O}_3$  thickness to  $8.1 \mu\text{m}$ . The strength at 1398 K exhibits a similar trend to that at 1273 K, whilst the variation is smaller, and its maximum is 128 MPa for a  $4.5 \mu\text{m}$   $\text{Al}_2\text{O}_3$  layer. (It may appear to increase monotonically except for the one annealed for 6 h.)

Figure 5(a) summarises the Young's modulus of porous  $\text{Cr}_2\text{AlC}$  annealed at 1473 K for different times in relation to the  $\text{Al}_2\text{O}_3$  thickness, obtained via compression tests at 298 K. The modulus shows a very similar trend as the compressive strength presented in Fig. 4(a), although its variation is much smaller than that of the strength. Figure 5(b) presents the Young's modulus vs compressive strength at 298 K. There appears to be a good correlation between the Young's modulus and compressive strength, whilst the fracture strain  $\varepsilon_f$  also correlates with the strength, where  $\varepsilon_f$  was determined using the strain corresponding to the maximum



stress.

Figure 6 presents the SEM images of fractured surface of oxidised porous  $\text{Cr}_2\text{AlC}$  annealed for 0, 3, and 20 h, respectively, fractured at 298 K ((a)-(c)) and 1273 K ((d)-(f)). The predominant fracture mode of porous  $\text{Cr}_2\text{AlC}$  is intergranular in all cases. There are very small  $\text{Al}_2\text{O}_3$  particles observable on the surface of intergranularly-fractured grains, as reported in literature [28], which exist already in the original material as can be seen in Fig. 1(d) as small dots. Some delaminations in the grains are also visible in the transgranularly-fractured grains, which are found in the vicinity of the  $\text{Al}_2\text{O}_3$  layers/domains. The cracks appear to propagate along the grain boundaries in the  $\text{Cr}_2\text{AlC}$  matrix and also connecting pores (internally covered with  $\text{Al}_2\text{O}_3$ ) in  $\text{Cr}_2\text{AlC}$  and  $\text{Cr}_7\text{C}_3$ . There are more transgranular fractures with rougher surfaces when fractured at high temperatures, especially for less-oxidised samples. No significant deformation of grains is observed. On the fracture surface of  $\text{Al}_2\text{O}_3$ , the columnar (inner) and equiaxial (outer) structures are confirmed, as reported for dense  $\text{Cr}_2\text{AlC}$  similarly [24]. Few delaminations of the  $\text{Al}_2\text{O}_3$  layer were observed after the fracture tests at any temperatures.

## 4. Discussion

### 4.1 Oxidation process of porous $\text{Cr}_2\text{AlC}$

Figure 7 illustrates schematically the oxidation process of porous  $\text{Cr}_2\text{AlC}$ , which is suggested on the basis of the SEM observations shown in Figs. 1 and 6. On the surface the as-prepared  $\text{Cr}_2\text{AlC}$  matrix (e.g. area A in Fig. 7(a)), has no oxidation layers at the beginning (Fig. 7(b)). As annealed, a dense and continuous  $\text{Al}_2\text{O}_3$  layer grows on the surfaces including pore surfaces, beneath which porous  $\text{Cr}_7\text{C}_3$  forms (Fig. 7(c)). As the  $\text{Al}_2\text{O}_3$  layer thickens, also the  $\text{Cr}_7\text{C}_3$  gets thicker and more porous with a higher rate (Fig. 7(d, e)). In the thin struts (e.g. area B in Fig. 7(a)), the oxidation proceeds in a similar way but with a faster rate of  $\text{Cr}_2\text{AlC}$  consumption due to higher specific surface area, which results in the breakage of  $\text{Al}_2\text{O}_3$  layers probably caused by a large volumetric expansion of porous  $\text{Cr}_7\text{C}_3$  (Fig. 7(d')), as can be observed in Fig. 1(e). The breakage of  $\text{Al}_2\text{O}_3$  layers leads to an oxygen inflow, which oxidises the  $\text{Cr}_7\text{C}_3$  into  $\text{Cr}_2\text{O}_3$ , followed by the spallation of  $\text{Cr}_2\text{O}_3$  and the formation of discontinuous  $\text{Al}_2\text{O}_3$  barriers/domains inside the

material (see Fig. 7(e')). At the end, the material consists mainly of  $\text{Al}_2\text{O}_3$ ,  $\text{Cr}_7\text{C}_3$ , and  $\text{Cr}_2\text{O}_3$  (Fig. 7(e)), where only a small amount of  $\text{Cr}_2\text{AlC}$  remains. For instance, the porous  $\text{Cr}_2\text{AlC}$  annealed at 1473 K for 3 h, 10 h, and 50 h has the microstructures illustrated in Fig. 7(c), (d, d'), and (e, e'), respectively. (This suggested mechanism appears to be representative when oxidised in the present temperature range, i.e., 1273 K to 1473 K, but not applicable to oxidation taking place at 1723 K or higher due to incongruent melting [1].)

The thickness of  $\text{Al}_2\text{O}_3$  layer increases monotonically with the annealing time and temperature as presented in Fig. 2. The microstructures with the same  $\text{Al}_2\text{O}_3$  thickness are similar to each other regardless of the annealing condition, which indicates that the development of the  $\text{Al}_2\text{O}_3$  layer might be represented by its thickness. The relationship between the time  $t$  and the  $\text{Al}_2\text{O}_3$  thickness  $\Delta h$  at each temperature can be approximated by a parabolic law [3],  $\rho\Delta h = (k_p t)^{1/2}$ , as shown in Fig. 8(a), where  $\rho$  is density of  $\text{Al}_2\text{O}_3$  ( $3.9 \times 10^3 \text{ kg/m}^3$  [35]) and  $k_p$  is an oxidation constant. Figure 8(b) is the Arrhenius plot of the oxidation constant, where  $k_p$  appears to follow a thermally-activated process. (Note here that the data of samples annealed at 1473 K for longer than 20 h are excluded due to the excessive oxidation.) The obtained activation energy for the  $\text{Al}_2\text{O}_3$  formation of porous  $\text{Cr}_2\text{AlC}$  was 346 kJ/mol, which is comparable to the one obtained for powder  $\text{Cr}_2\text{AlC}$  using thermogravimetric analysis (297 kJ/mol) [34]. The increase of the  $\text{Al}_2\text{O}_3$  thickness  $\Delta h$  with annealing time measured at ambient temperature can thus be expressed by the following relationship:

$$\rho\Delta h = \{16677 t \exp(-41632/T)\}^{1/2} \quad [\text{kg/m}^2] \quad (1),$$

where the coefficient of determination  $R^2 = 0.9998$  for Eq. (1) and  $R^2 = 0.936\text{--}0.996$  for the original parabolic curve fittings (Fig. 8). (The relatively low  $R^2$  values could be mostly attributed to the large variations of the measured thickness shown in Fig. 2.) It should be noted that, if a cubic law  $\rho\Delta h = (k_{pt})^{1/3}$  is applied, the following relationship results:

$$\rho\Delta h = \{2.66 \times 10^6 t \exp(-54423/T)\}^{1/3} \quad [\text{kg/m}^2] \quad (2),$$

where  $R^2=0.9955$  for Eq. (2) and  $R^2= 0.932\text{--}0.986$  for original cubic curve fittings. These results suggest that the parabolic law appears to provide a better fitting than the cubic law in the present case, although the

exact oxidation kinetics of  $\text{Cr}_2\text{AlC}$  is considered to be more complex compared to other Al-based MAX phases and not to follow simple parabolic or cubic law [3].

#### *4.2. Mechanical Properties of oxidised porous $\text{Cr}_2\text{AlC}$*

##### *4.2.1. Room Temperature*

As shown in Figs. 4 and 5, the compressive strength and Young's modulus at 298 K have their maximum values (150 MPa and 63 GPa, respectively) for a thin  $\text{Al}_2\text{O}_3$  layer (c.a. 2.5  $\mu\text{m}$ ). However, further growth of the  $\text{Al}_2\text{O}_3$  layer (up to 8  $\mu\text{m}$ ) rather deteriorates the improvements. It can be considered that the continuous and cohesive  $\text{Al}_2\text{O}_3$  layer formed on  $\text{Cr}_2\text{AlC}$  via porous  $\text{Cr}_7\text{C}_3$  plays an important role in the improvement of the mechanical properties, as has been seen for the high-temperature creep resistance reported in the previous study [26].

Figure 9 illustrates the fracture modes of the oxidised porous  $\text{Cr}_2\text{AlC}$  with crack propagation paths, which are derived on the basis of the SEM observations of cross-sections and fracture surfaces. As a general rule, the predominant fracture mode of porous  $\text{Cr}_2\text{AlC}$  is intergranular as verified for the dense  $\text{Cr}_2\text{AlC}$  [32], whilst a transgranular fracture is additionally observed in grains that are constrained by the  $\text{Al}_2\text{O}_3$  layers/domains or material boundaries (Fig. 9(a)). Non-oxidised porous  $\text{Cr}_2\text{AlC}$  fractures intergranularly, possibly starting from defects such as very small  $\text{Al}_2\text{O}_3$  particles at grain boundaries. Slightly-oxidised one fractures in the same way, where the crack propagation starting from the grain boundaries of  $\text{Cr}_2\text{AlC}$  could be hindered by the  $\text{Al}_2\text{O}_3$  layer (Fig. 9(b)), resulting in the reinforcement of the material. If annealed longer, the  $\text{Cr}_7\text{C}_3$  layers becomes more porous with larger pore sizes, where the inner surface of pores is also oxidised, where the cracks appear to initiate from / propagate through these pores due to stress concentrations (Fig. 9(c)) [22]. An excessive oxidation causes the breakages of  $\text{Al}_2\text{O}_3$ , followed by a material decomposition as explained in Fig. 7, which seems to result in a weakening of the mechanical properties due to multiple possible crack paths, i.e., (Fig. 9(d)). Cracks connecting the pores are frequently observed in the vicinity of material boundaries (i.e.  $\text{Cr}_2\text{O}_3/\text{Cr}_7\text{C}_3$  and  $\text{Cr}_7\text{O}_3/\text{Cr}_2\text{AlC}$ ). Therefore, a slight oxidation can improve the mechanical properties, especially the strength, due to the dense and

cohesive  $\text{Al}_2\text{O}_3$  layer preventing the crack to propagate from inside; however, an excessive oxidation causes the breakage of  $\text{Al}_2\text{O}_3$ , followed by the decomposition of  $\text{Cr}_2\text{AlC}$ , which deteriorates the strength improvements.

For further discussion, the variation of mechanical properties was estimated by a simple theoretical model: The properties of porous  $\text{Cr}_2\text{AlC}$  with  $\text{Al}_2\text{O}_3$  and  $\text{Cr}_7\text{C}_3$  layers might be roughly expressed by a Voigt model,  $X = \sum X_i \phi_i$  ( $i = 1 \sim 3$ ) [37], where  $X_i$  is property (Young's modulus  $E$  or compressive strength  $\sigma_c$ ) of each phase,  $\phi_i$  is volume fraction ( $= V_i/V$ , where  $V_i$  is volume of each phase and  $V$  is the total volume), and  $i$  is material index (1 = porous  $\text{Cr}_2\text{AlC}$ , 2 = dense  $\text{Al}_2\text{O}_3$ , 3 = porous  $\text{Cr}_7\text{C}_3$ , hereafter). The Voigt model was chosen in this study, as this is one of the simplest models which can predict reinforcements. For the  $\text{Al}_2\text{O}_3$  phase ( $i = 2$ ), Young's modulus and compressive strength are 340 GPa and 2500 MPa [35], respectively, and the variation of volume fraction was estimated based on Eq. (1) assuming an average pore size of 215  $\mu\text{m}$  [16]. For the porous  $\text{Cr}_2\text{AlC}$  phase ( $i = 1$ ), the apparent volume including pores is assumed to be constant, whereas its porosity is considered to increase if annealed (considering a volume decrease in the microstructure) following a chemical reaction (i.e., the formation of 1 mol of  $\text{Al}_2\text{O}_3$  costing 2 mol of  $\text{Cr}_2\text{AlC}$ ). The variation of mechanical properties of  $\text{Cr}_2\text{AlC}$  with increasing porosity at 298 K is estimated on the basis of preliminary experimental results shown in Fig. 10. (The modulus and strength were obtained in identical compressive tests using specimens with the porosity of 2%, 53%, and 75%. Details on the used materials can be found in our previous studies [26][27].) For porous  $\text{Cr}_7\text{C}_3$  ( $i = 3$ ), the apparent volume (including pores) is roughly assumed to increase four times larger than the volume of  $\text{Al}_2\text{O}_3$ , which leads to a total volume expansion that agrees with the one experimentally observed, whilst its mechanical properties are to be variables. Table 1 summarises the properties used for the estimations.

Figure 11 presents the variation of mechanical properties as estimated by the Voigt model with  $\text{Cr}_7\text{C}_3$  properties ( $X_3$ ) as variables. (Here, the properties of oxidised porous  $\text{Cr}_2\text{AlC}$  with  $\text{Al}_2\text{O}_3$  thicker than 5.5  $\mu\text{m}$  are not discussed since the microstructure is different due to the excessive oxidation.) In the early oxidation stage, i.e., when the  $\text{Al}_2\text{O}_3$  thickness  $\Delta h \leq 3 \mu\text{m}$ , the increase of total Young's modulus  $E$  can be explained

well by the reinforcement of  $\text{Al}_2\text{O}_3$  layer as shown in Fig. 11(a), where the porous  $\text{Cr}_7\text{C}_3$  ( $E_3 = 165$  GPa) is not yet dominant in the structure. If annealed longer, i.e., when  $\Delta h \geq 3 \mu\text{m}$ , more porous  $\text{Cr}_7\text{C}_3$  with lower modulus ( $E_3 = 65\sim 110$  GPa) forms and becomes more dominant in the structure, which appears to result in a decrease of the total modulus. The compressive strength shown in Fig. 11(b) is significantly enhanced by the  $\text{Al}_2\text{O}_3$  layer, as the strength of  $\text{Al}_2\text{O}_3$  is much higher than porous  $\text{Cr}_2\text{AlC}$ . For  $\Delta h = 3 \mu\text{m}$ , the maximum strength of 153 MPa can be modelled using the  $\sigma_{c3} = 280$  MPa. For  $\Delta h \geq 3 \mu\text{m}$ , where porous  $\text{Cr}_7\text{C}_3$  becomes dominant, the decreasing of  $\sigma_{c3}$  (e.g.  $\sigma_{c3}$  as low as 10 MPa) does not predict the decrease of the total strength unlike  $E$ , because the strength  $\text{Al}_2\text{O}_3$  is much higher than that of the others. This suggests that the decrease of total strength for  $\Delta h \geq 3 \mu\text{m}$  might be attributed to the breakage of the continuous  $\text{Al}_2\text{O}_3$  layers.

Therefore, the moderate variation of modulus in relation to  $\text{Al}_2\text{O}_3$  thickness is attributed to the combination of volume fractions of  $\text{Al}_2\text{O}_3$  and porous  $\text{Cr}_7\text{C}_3$ , whereas the considerable variation of strength can be attributed to the continuity of the cohesive  $\text{Al}_2\text{O}_3$  layer. Although the present property estimations contain various assumptions due to a number of uncertain parameters, it is helpful to understand the variation of mechanical properties with respect to oxidation.

#### 4.2.2. High Temperature

A mechanical behaviour with plasticity was observed at 1273 K only for less-oxidised specimens and at 1398 K for all the specimens. The porous  $\text{Cr}_2\text{AlC}$  specimens that did not show a large plastic deformation fracture in a brittle manner, whereas the plastically-deformed ones tend to collapse. The porous  $\text{Cr}_2\text{AlC}$  teste at high temperatures has more intergranular fracture with rougher fracture surfaces, compared to the ones tested at 298 K. Transgranular fracture with delaminations in the grains appears mostly just beneath the  $\text{Al}_2\text{O}_3$ . The rough surface, especially found for less-oxidised specimens, can be attributed to dimples caused by a plastic deformation around very small  $\text{Al}_2\text{O}_3$  particles at grain boundaries, as illustrated in Fig. 9(e), which could lead to the macroscopically-observed plastic deformation shown in Fig. 3. (It is worth noting that this result implies that less segregation of  $\text{Al}_2\text{O}_3$  at the grain boundaries would suppress the

plastic deformation at high temperatures, leading to an increase of the brittle-plastic transition temperature, which requires however further verification.) In addition, the small spikes observed in Fig. 3, which are found only during the plastic deformation at high temperature, might be related to further oxidation probably followed by the breakage of the oxidation layer during the deformation, as less annealed samples at higher temperatures show these spikes more frequently.

As shown in Fig. 4, the sample annealed at 1473 K for 3 h (with  $\Delta h = 2.5 \mu\text{m}$ ) has significantly improved mechanical properties when measured at 298 K, whereas prominent but smaller improvements are observed with thicker  $\text{Al}_2\text{O}_3$  ( $\Delta h = \text{c.a. } 5 \mu\text{m}$ ) at 1273 K and 1398 K. To understand this apparent difference between the behaviour at room and high temperatures, additional compression tests were performed in the temperature range from 298 K to 1398 K, in particular around 1273 K, only for porous  $\text{Cr}_2\text{AlC}$  annealed at 1473 K for 3 h ( $\Delta h = \text{c.a. } 2.5 \mu\text{m}$ ). Figure 12 shows the compressive strength of porous  $\text{Cr}_2\text{AlC}$  annealed at 1473 K for 3 h as a function of temperature, where the strength of porous  $\text{Cr}_2\text{AlC}$  annealed at 1473 K for 0, 10, and 50 h are shown for comparison. (Note that the small growth of the  $\text{Al}_2\text{O}_3$  layer during the test is not considered here.) The improved strength is retained from 298 K to 1248 K (with only a 10% of variation), where all the samples fracture in a brittle manner, whereas it drops sharply around 1273 K, followed by a slight recovery at 1398 K. For dense  $\text{Cr}_2\text{AlC}$ , mechanical behaviour with obvious plasticity was observed above 1173 K in a four-point bending test [32], accompanied by an abrupt decrease of the flexural strength. It was concluded that the brittle-to-plastic transition temperature was between 1173 and 1273 K [32]. Therefore, although the mechanical properties of the porous  $\text{Cr}_2\text{AlC}$  matrix without oxidation should decrease above the temperature of 1173 K, the pre-formed  $\text{Al}_2\text{O}_3$  ( $\Delta h = 2.5 \mu\text{m}$ ) leads to a retained strength of the porous  $\text{Cr}_2\text{AlC}$  up to 1273 K. However, when the strength of  $\text{Cr}_2\text{AlC}$  matrix becomes too low above 1173 K, it requires a thicker  $\text{Al}_2\text{O}_3$  layer ( $\Delta h = 5 \mu\text{m}$ ) to retain a superior strength. At high temperatures, the decomposition of the material does not degrade the strength much, probably because the amount of  $\text{Al}_2\text{O}_3$  with its superior properties plays an important role.

#### *4.3. Recommended lifetime*

On the basis of the present experimental results, a safety criterion of porous Cr<sub>2</sub>AlC for application at elevated temperature is discussed in the following from a mechanical point of view.

When as-prepared (i.e., non-oxidised) porous Cr<sub>2</sub>AlC is used at elevated temperature, it will be gradually oxidised. It was observed that some oxidation can monotonically improve the mechanical properties of porous Cr<sub>2</sub>AlC, whereas an excessive oxidation could ruin the improvement. The variation of mechanical properties during oxidation (at 1473 K and lower) can be attributed to the microstructural changes illustrated in Figs. 7 and 8, which can be represented by the Al<sub>2</sub>O<sub>3</sub> thickness determined by Eq. (1). For instance, at operation temperature 1273 K, the initial compressive strength of porous Cr<sub>2</sub>AlC (almost) without oxidation is about 58 MPa (as shown in Fig. 4(b)), and it is expected to monotonically increase during usage at 1273 K until the thickness of the Al<sub>2</sub>O<sub>3</sub> layer reaches ~ 5 µm, which can be obtained after ~1008 h according to Eq. (1). In other words, as-prepared porous Cr<sub>2</sub>AlC can be used without property degradation (rather with some property improvement) until 1008 h at 1273 K. Below 1243 K, the mechanical property will be retained or even improved until the Al<sub>2</sub>O<sub>3</sub> layer grows to ~2.5 µm, assuming that mechanical properties remain unchanged in the temperature range from 298 K to 1243 K, as shown in Fig. 12.

Figure 13 summarises the recommended maximum operation times  $t_{app}$  without mechanical property degradation at operation temperatures from 1100 K to 1400 K, which can be determined by

$$t_{app} = (\rho \Delta h_x)^2 \exp(41632 / T) / 16677 \quad [s] \quad (3),$$

where  $\Delta h_x$  is the thickness of Al<sub>2</sub>O<sub>3</sub> where the mechanical properties (i.e., here compressive strength) show their maxima, which is assumed to be 2.5 µm for  $T \leq 1273$  K and 5 µm for  $T \geq 1273$  K, respectively. It should be noted that the material would deform plastically at temperatures above 1173 K.

## 5. Conclusion

Oxidation kinetics and mechanical behaviour of Cr<sub>2</sub>AlC were investigated in this study. The porous Cr<sub>2</sub>AlC with a porosity of 53% was oxidised at different temperature, and the microstructures of the

oxidised porous  $\text{Cr}_2\text{AlC}$  specimens were examined. Uniaxial compression tests were performed at various temperatures using porous  $\text{Cr}_2\text{AlC}$  oxidised at 1473 K to characterize the mechanical properties.

Overall the oxidation of porous  $\text{Cr}_2\text{AlC}$  is similar to the oxidation of its dense counterpart: A continuous and cohesive  $\text{Al}_2\text{O}_3$  layer forms on the  $\text{Cr}_2\text{AlC}$  matrix, beneath which porous  $\text{Cr}_7\text{C}_3$  forms. The oxidation mechanism can be roughly expressed by a parabolic law. However, an excessive oxidation takes place, first in thin struts, where the formed  $\text{Al}_2\text{O}_3$  layer breaks, followed by an oxygen inflow and decomposition of the inner material. This excessive oxidation in thin struts appears to start when the thickness of the  $\text{Al}_2\text{O}_3$  layer exceeds 2.5  $\mu\text{m}$ .

At room temperature (298 K), non-oxidised porous  $\text{Cr}_2\text{AlC}$  fractures intergranularly, possibly with crack initiations from very small  $\text{Al}_2\text{O}_3$  particles at grain boundaries. Constrained grains tend to fracture transgranularly with delaminations. Slight oxidation significantly improves the mechanical properties, especially the compressive strength, as the  $\text{Al}_2\text{O}_3$  layer formed on the surface can prevent the initiated cracks to propagate from inside outward. However, an excessive oxidation (with the  $\text{Al}_2\text{O}_3$  layer thicker than 2.5  $\mu\text{m}$ ) deteriorates the improvement in the strength, which can be explained by a breakage of the  $\text{Al}_2\text{O}_3$  layer at thin struts followed by a material decomposition.

At elevated temperatures (1273 K and 1398 K), non-oxidised porous  $\text{Cr}_2\text{AlC}$  fractures intergranularly accompanied with a plastic deformation around very small  $\text{Al}_2\text{O}_3$  particles at grain boundaries, which results in a macroscopic plastic deformation. Although the predominant fracture mode of slightly-oxidised porous  $\text{Cr}_2\text{AlC}$  is also intergranular, a thicker  $\text{Al}_2\text{O}_3$  layer (~5  $\mu\text{m}$ ) is required to reinforce the material, since the  $\text{Cr}_2\text{AlC}$  matrix softens and gets weaker at high temperatures. The brittle-to-plastic transition temperature appears to be slightly raised by the  $\text{Al}_2\text{O}_3$  layer with a thickness of 2.5  $\mu\text{m}$  from 1173 to 1273 K for non-oxidised, dense  $\text{Cr}_2\text{AlC}$ .

Lastly, a safety criterion, i.e., a maximum operating time at high temperature, is suggested on the basis of the oxidation and fracture mechanisms discussed above: for example, the non-oxidised porous  $\text{Cr}_2\text{AlC}$  can be used at 1273 K for up to 1008 h with no property degradation but rather with some improvement.



## **ACKNOWLEDGEMENTS**

This work is supported by a Bilateral Program between the Japan Society for the Promotion of Science and the German Academic Exchange Service (JSPS/DAAD) with the project number JPJSBP120193505 for JSPS, 57457777 for DAAD, respectively. Jesus Gonzalez-Julian thanks the financial support by the Germany's Federal Ministry of Education and Research ("Bundesministerium für Bildung und Forschung") under the MAXCOM project (03SF0534).

## References

- [1] M.W. Barsoum, MAX Phases. Properties of machinable ternary carbides and nitrides, Wiley VCH, 2013.
- [2] B.M. Radovic, M.W. Barsoum, MAX phases : Bridging the gap between metals and ceramics, Am. Ceram. Soc. Bull. 92 (2013) 20–27.
- [3] D.J. Tallman, B. Anasori, M.W. Barsoum, A critical review of the oxidation of  $\text{Ti}_2\text{AlC}$ ,  $\text{Ti}_3\text{AlC}_2$  and  $\text{Cr}_2\text{AlC}$  in air, Mater. Res. Lett. 1 (2013) 115–125.
- [4] J.L. Smialek, Oxygen diffusivity in alumina scales grown on Al-MAX phases, Corros. Sci. 91 (2015) 281–286.
- [5] J. Gonzalez-Julian, T. Go, D.E. Mack, R. Vaßen, Environmental resistance of  $\text{Cr}_2\text{AlC}$  MAX phase under thermal gradient loading using a burner rig, J. Am. Ceram. Soc. 101 (2018) 1841–1846.
- [6] J.L. Smialek, Environmental resistance of a  $\text{Ti}_2\text{AlC}$ -type MAX phase in a high pressure burner rig, J. Eur. Ceram. Soc. 37 (2017) 23–34..
- [7] M.W. Barsoum, M. Radovic, Elastic and mechanical properties of the MAX phases, Annu. Rev. Mater. Res. 41 (2011) 195–227.
- [8] Z. Wang, J. Sund, B. Xua, Y. Liua, P. Kea, A. Wang, Reducing the self-healing temperature of  $\text{Ti}_2\text{AlC}$  MAX phase coating by substituting Al with Sn, J. Eur. Ceram. Soc. 40 (2020) 197–201.
- [9] P. Eklund, M. Beckers, U. Jansson, H. Högberg, L. Hultman, The  $\text{M}_{n+1}\text{AX}_n$  phases: Materials science and thin-film processing, Thin Solid Films. 518 (2010) 1851–1878.
- [10] J. Gonzalez-Julian, J. Llorente, M. Bram, M. Belmonte, O. Guillon, Novel  $\text{Cr}_2\text{AlC}$  MAX-phase/ $\text{SiC}$  fiber composites: Synthesis, processing and tribological response, J. Eur. Ceram. Soc. 37 (2017).
- [11] M. Potoczek, E. Guzi de Moraes, P. Colombo,  $\text{Ti}_2\text{AlC}$  foams produced by gel-casting, J. Eur. Ceram. Soc. 35 (2015) 2445–2452.
- [12] T. Fey, M. Stumpf, A. Chmielarz, P. Colombo, P. Greil, M. Potoczek, Microstructure, thermal conductivity and simulation of elastic modulus of MAX-phase ( $\text{Ti}_2\text{AlC}$ ) gel-cast foams, J. Eur. Ceram. Soc. 38 (2018) 3424–3432.

- [13] B. Velasco, E. Gordo, L. Hu, M. Radovic, S.A. Tsipas, Influence of porosity on elastic properties of  $\text{Ti}_2\text{AlC}$  and  $\text{Ti}_3\text{SiC}_2\text{MAX}$  phase foams, *J. Alloys Compd.* 764 (2018) 24–35.
- [14] B. Velasco, E. Gordo, S.A. Tsipas, MAX phase  $\text{Ti}_2\text{AlC}$  foams using a leachable space-holder material, *J. Alloys Compd.* 646 (2015) 1036–1042.
- [15] C.R. Bowen, T. Thomas, Macro-porous  $\text{Ti}_2\text{AlC}$  MAX-phase ceramics by the foam replication method, *Ceram. Int.* 41 (2015) 12178–12185.
- [16] J. Gonzalez-Julian, S. Onrubia, M. Bram, C. Broeckmann, R. Vaßen, O. Guillon, High temperature oxidation and compressive strength of  $\text{Cr}_2\text{AlC}$  MAX phase foams with controlled porosity, *J. Am. Ceram. Soc.* 101 (2018) 542–552.
- [17] S. Karimi, T. Go, R. Vaßen, J. González-Julián,  $\text{Cr}_2\text{AlC}$  MAX phase foams by replica method, *Mater. Lett.* 240 (2019) 271–274.
- [18] J.L. Smialek, S. Gray, Type II Hot corrosion screening tests of a  $\text{Cr}_2\text{AlC}$  MAX phase compound, *Oxid. Met.* 90 (2018) 555–570.
- [19] J.L. Smialek, Oxidation of  $\text{Al}_2\text{O}_3$  Scale-forming MAX phases in turbine environments, *Metall. Mater. Trans. A Phys. Metall. Mater. Sci.* (2017) 1–11.
- [20] J.L. Smialek, J.A. Nesbitt, T.P. Gabb, A. Garg, R.A. Miller, Hot corrosion and low cycle fatigue of a  $\text{Cr}_2\text{AlC}$ -coated superalloy, *Mater. Sci. Eng. A.* 711 (2018) 119–129.
- [21] Z. Wanga, G. Ma, L. Liu, L. Wang, P. Ke, Q. Xue, A. Wang, High-performance  $\text{Cr}_2\text{AlC}$  MAX phase coatings: Oxidation mechanisms in the 900–1100°C temperature range, *Corrosion Sci.* 167 (2020) 108492.
- [22] D.B. Lee, T.D. Nguyen, J.H. Han, S.W. Park, Oxidation of  $\text{Cr}_2\text{AlC}$  at 1300 °C in air, *Corros. Sci.* 49 (2007) 3926–3934.
- [23] S. Li, X. Chen, Y. Zhou, G. Song, Influence of grain size on high temperature oxidation behavior of  $\text{Cr}_2\text{AlC}$  ceramics, *Ceram. Int.* 39 (2013) 2715–2721.
- [24] H.J. Yang, Y.T. Pei, J.T.M. De Hosson, Oxide-scale growth on  $\text{Cr}_2\text{AlC}$  ceramic and its consequence for self-healing, *Scr. Mater.* 69 (2013) 203–206.

- [25] A.S. Farle, C. Kwakernaak, S. van der Zwaag, W.G. Sloof, A conceptual study into the potential of  $Mn+1AX_n$ -phase ceramics for self-healing of crack damage, *J. Eur. Ceram. Soc.* 35 (2015) 37–45.
- [26] W. Araki, J. Gonzalez-Julian, J. Malzbender, High temperature compressive creep of dense and porous  $Cr_2AlC$  in air, *J. Eur. Ceram. Soc.* 39 (2019) 3660–3667.
- [27] J. Gonzalez-Julian, S. Onrubia, M. Bram, O. Guillon, Effect of sintering method on the microstructure of pure  $Cr_2AlC$  MAX phase ceramics, *J. Ceram. Soc. Japan.* 124 (2016) 415–420.
- [28] W. Tian, P. Wang, G. Zhang, Y. Kan, and Y. Li, Mechanical properties of  $Cr_2AlC$  ceramics, *J. Am. Ceram. Soc.*, 90 (2007) 1663–1666.
- [29] J.M. Schneider, D.P. Sigumonrong, D. Music, C. Walter, J. Emmerlich, R. Iskandar and J. Mayer, Elastic properties of  $Cr_2AlC$  thin films probed by nanoindentation and ab initio molecular dynamics, *Scripta Mater.* 57 (2007) 1137–1140.
- [30] G. Ying, X. He, M. Li, S. Du, W. Han, and F. He, Effect of  $Cr_7C_3$  on the mechanical, thermal, and electrical properties of  $Cr_2AlC$ , *J. Alloys Compd.* 509 (2011) 8022– 8027.
- [31] H. Li, S. Li, and Y. Zhou, Cyclic thermal shock behaviour of a  $Cr_2AlC$  ceramic, *Mater. Sci. Eng. A* 607 (2014) 525–529.
- [32] W. Tian, Z. Sun, Y. Du, and H. Hashimoto, Mechanical properties of pulse discharge sintered  $Cr_2AlC$  at 25–1000 °C, *Materials Letters* 63 (2009) 670–672.
- [33] H. Gao, R. Benitez, W. Son, R. Arroyave, and M. Radovic, Structural, physical and mechanical properties of  $Ti_3(Al_{1-x}Ti_xSi_x)C_2$  solid solution with  $x=0-1$ , *Mater. Sci. & Eng. A* 676 (2016) 197–208.
- [34] Y. Bai, X. He, C. Zhu, and G. Chen, Microstructures, electrical, thermal, and mechanical properties of bulk  $Ti_2AlC$  synthesized by self-propagating high-temperature combustion synthesis with pseudo hot isostatic pressing, *J. Am. Ceram. Soc.* 95 (2012) 358–364.
- [35] Matweb, <http://www.matweb.com/search/DataSheet>, Overview–Alumina, 98%,  $Al_2O_3$  (Mar 2020).
- [36] Z.J. Lin, M.S. Li, J.Y. Wang, Y.C. Zhou, High-temperature oxidation and hot corrosion of  $Cr_2AlC$ , *Acta Mater.* 55 (2007) 6182–6191.
- [37] W. Voigt, Ueber die Beziehung zwischen den beiden Elasticitätsconstanten isotroper Körper, *Ann.*

Phys. 274 (1889) 573–587.

## Captions

**Table 1** Parameters used for the property estimations in Fig. 11.

**Figure 1** Cross-sectional SEM images of porous  $\text{Cr}_2\text{AlC}$  annealed 1473 K for different hours: (a) 3 h, (b) 10 h, and (c) 50 h at lower magnification, and (d) 3 h, (e) 10 h, and (f) 50 h at higher magnifications. Each area is assigned to  $\text{Cr}_7\text{C}_3$ ,  $\text{Cr}_2\text{AlC}$ ,  $\text{Cr}_2\text{O}_3$ ,  $\text{Al}_2\text{O}_3$ , and pore (embedding resin), respectively, from the brightest colour.

**Figure 2** Thickness of  $\text{Al}_2\text{O}_3$  layer formed on porous  $\text{Cr}_2\text{AlC}$  annealed at different temperatures and times.

**Figure 3** Mechanical behaviours of porous  $\text{Cr}_2\text{AlC}$  annealed at 1473 K for different hours, obtained in the uniaxial compression test at different temperatures: (a) 298 K, (b) 1273 K, and (c) 1398 K.

**Figure 4** Compressive strength and  $\text{Al}_2\text{O}_3$  thickness of porous  $\text{Cr}_2\text{AlC}$  annealed at 1473 K for different hours, obtained in the uniaxial compression test at different temperatures: (a) 298 K, (b) 1273 K, and (c) 1398 K. The symbol \* represents the specimen annealed at 1373 K for 1 h. The symbols  $\circ$  and  $\bullet$  express predominant mechanical behaviours:  $\circ$  is for brittle fracture, whilst  $\bullet$  is for plastic deformation.

**Figure 5** Young's modulus of porous  $\text{Cr}_2\text{AlC}$  annealed at 1473 K for different hours, obtained in the uniaxial compression tests at 298 K with relation to (a)  $\text{Al}_2\text{O}_3$  thickness and (b) compressive strength at 298 K. The symbol \* represents the specimen annealed at 1373 K for 1 h. The inset in (b) shows the strength vs the fracture strain relationship.

**Figure 6** Fracture surface of porous  $\text{Cr}_2\text{AlC}$  annealed at 1473 K for different hours tested in the uniaxial compression at different temperatures: (a-c) and (d-f) are fractured at 298 K and 1273 K respectively,

whilst (a)(d), (b)(e), (c)(f) are annealed for 0, 3, and 20 h, respectively. The white and grey arrows indicate the cracks along grain boundaries and the delaminations in grains, respectively.

**Figure 7** Oxidation mechanism of porous  $\text{Cr}_2\text{AlC}$ : (a) General view, (b)-(e) oxidation process on the surface of  $\text{Cr}_2\text{AlC}$  (e.g. area A in (a)), and (d')(e') oxidation process around thin strut (e.g. area B in (a)), corresponding stage to (d) and (e)).

**Figure 8**  $\text{Al}_2\text{O}_3$  growth on porous  $\text{Cr}_2\text{AlC}$  oxidised under different conditions: (a) Approximations by the parabolic law and (b) Arrhenius plot of oxidation constant.

**Figure 9** Fracture mode with crack propagation path in oxidised porous  $\text{Cr}_2\text{AlC}$ : (a)  $\text{Al}_2\text{O}_3$  particles at the grain boundaries and transgranular fractures with delaminations (shown as striped patterns) in the constrained grains, (b) intergranular fracture in a slightly-oxidised sample, (c) in a more oxidised sample, (d) in an excessively-oxidised sample (corresponding to Fig. 7(e')), and (e) intergranular fracture with dimple formations at high temperatures. The dashed lines indicate possible crack propagation paths.

**Figure 10** Mechanical properties of  $\text{Cr}_2\text{AlC}$  with different porosities obtained in the uniaxial compression test at 298 K and the approximations.

**Figure 11** Predictions of mechanical properties of oxidised porous  $\text{Cr}_2\text{AlC}$  at 298 K: (a) Young's modulus and (b) compressive strength.

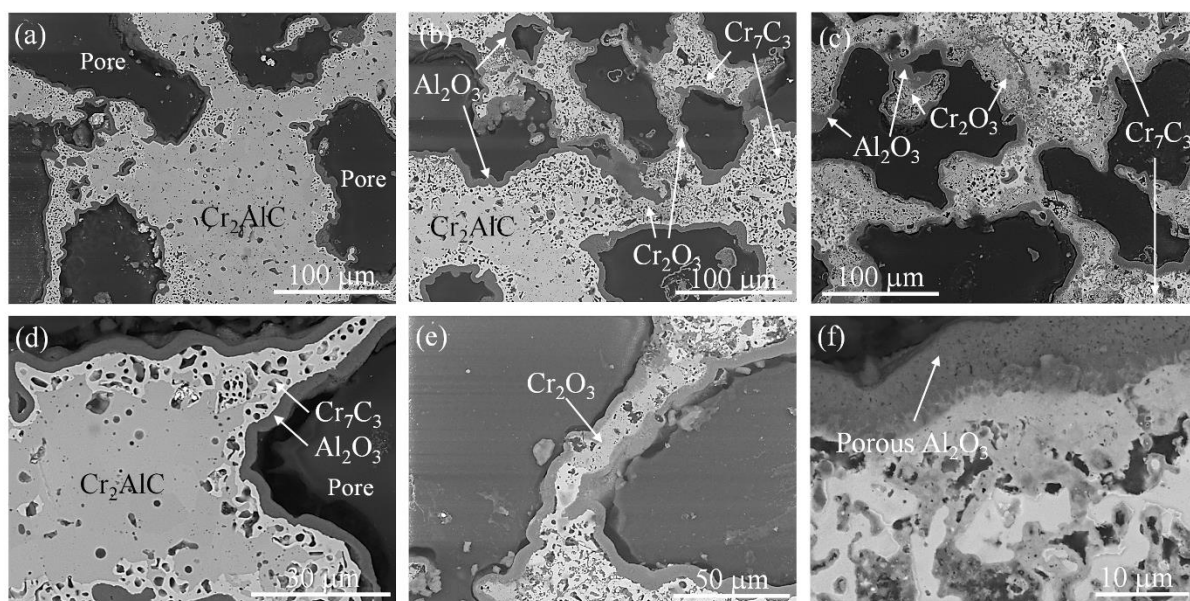
**Figure 12** Compressive strength of porous  $\text{Cr}_2\text{AlC}$  annealed at 1473 K for 3 h as a function of temperature from 298 K to 1398 K. The strength of porous  $\text{Cr}_2\text{AlC}$  annealed at 1473 K for 0, 10, and 50 h are shown for comparison. The open and filled symbols represent brittle fracture and plastic deformation, respectively.

**Figure 13** Recommended operating condition with Al<sub>2</sub>O<sub>3</sub> thickness. The optimum Al<sub>2</sub>O<sub>3</sub> thickness is assumed to be 2.5 μm for the temperature  $T \leq 1273$  K and 5 μm for  $T \geq 1273$  K, respectively, whilst the BRT (the brittle-to-plastic transition temperature) is 1273 K for the Al<sub>2</sub>O<sub>3</sub> thickness of 2.5 μm.

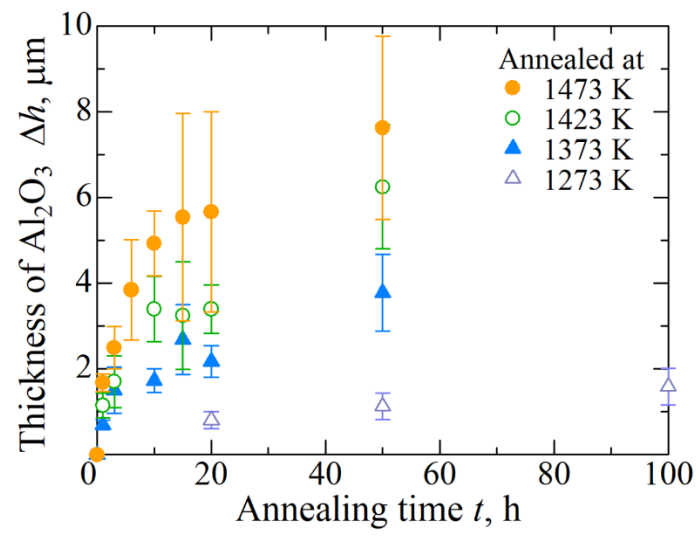


Table 1 Parameters used for the property estimations in Fig. 11.

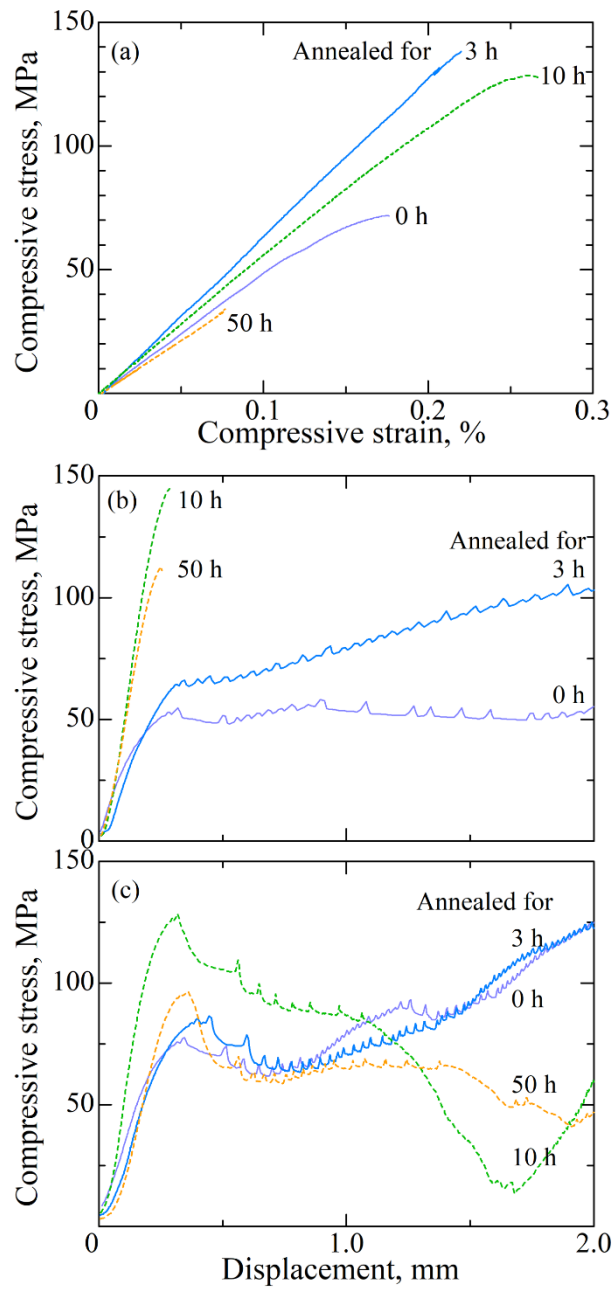
Material	Index $i$	Porosity $p$	Volume $V_i$	Young's modulus $E_i$ , GPa	Compressive strength $\sigma_{ci}$ , MPa
Cr <sub>2</sub> AlC	1	Porous ( $\geq 53\%$ )	Apparently constant	$E_1 = 340 \exp(-3.62p)$ (Fig. 10)	$\sigma_{c1} = 1370 \exp(-5.46p)$ (Fig. 10)
Al <sub>2</sub> O <sub>3</sub>	2	Dense	Eq. (1)	340	2500
Cr <sub>7</sub> C <sub>3</sub>	3	Porous	Four times $V_2$	Variable	Variable



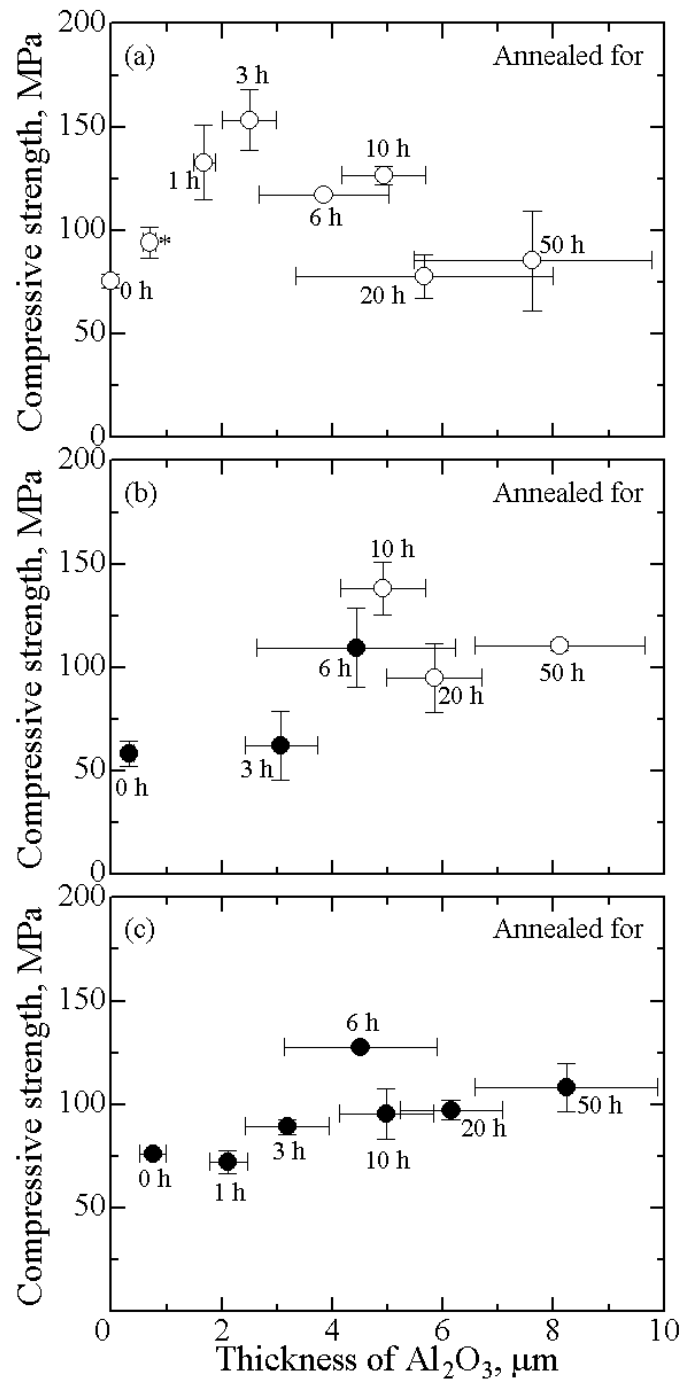
**Figure 1** Cross-sectional SEM images of porous  $\text{Cr}_2\text{AlC}$  annealed 1473 K for different hours: (a) 3 h, (b) 10 h, and (c) 50 h at lower magnification, and (d) 3 h, (e) 10 h, and (f) 50 h at higher magnifications. Each area is assigned to  $\text{Cr}_7\text{C}_3$ ,  $\text{Cr}_2\text{AlC}$ ,  $\text{Cr}_2\text{O}_3$ ,  $\text{Al}_2\text{O}_3$ , and pore (embedding resin), respectively, from the brightest colour.



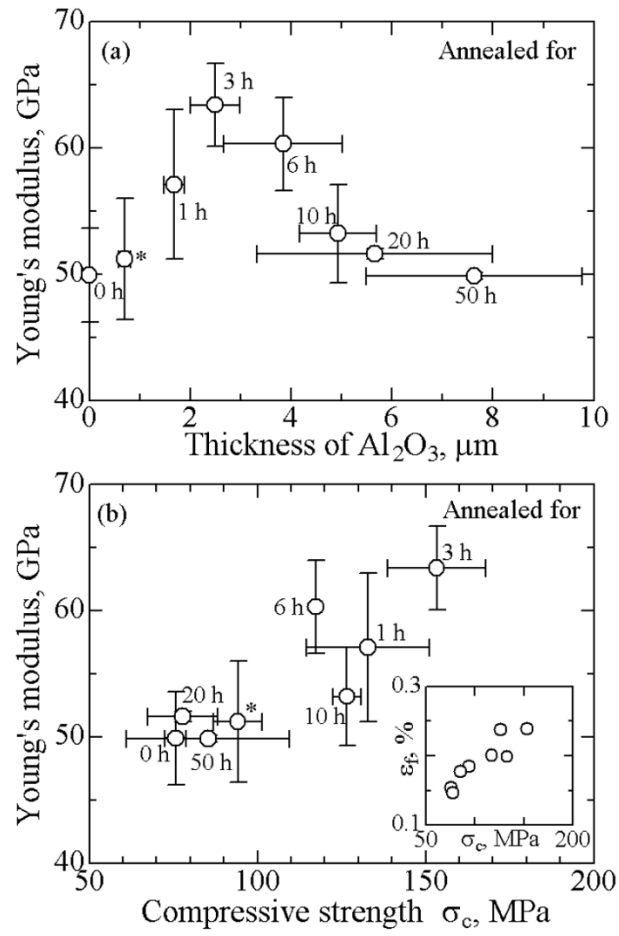
**Figure 2** Thickness of  $\text{Al}_2\text{O}_3$  layer formed on porous  $\text{Cr}_2\text{AlC}$  annealed at different temperatures and times.



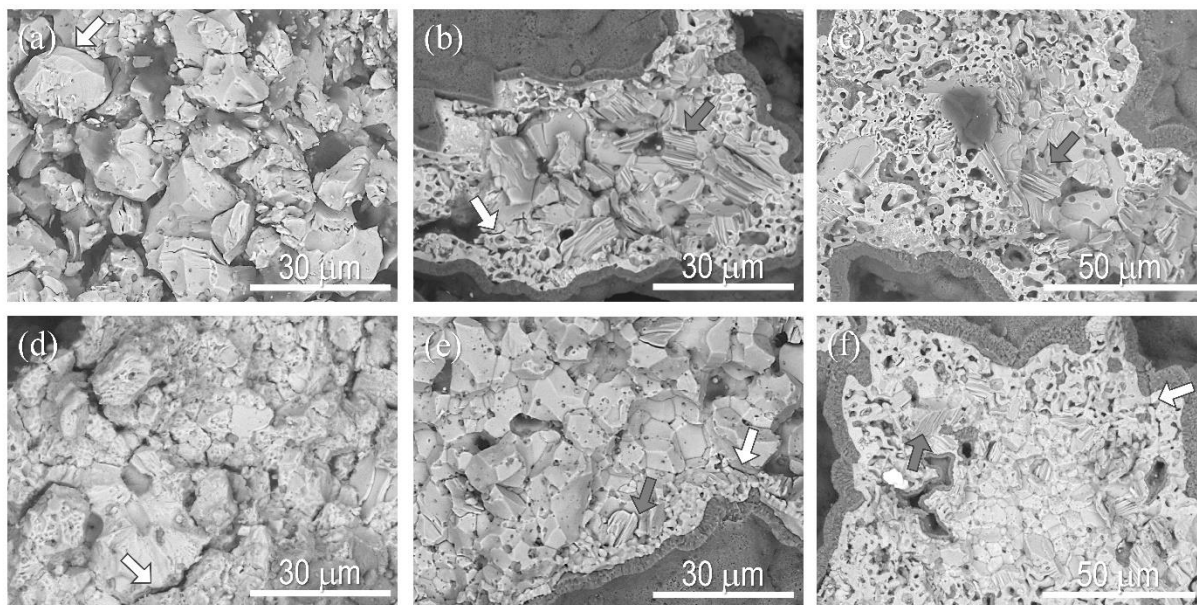
**Figure 3** Mechanical behaviours of porous  $\text{Cr}_2\text{AlC}$  annealed at 1473 K for different hours, obtained in the uniaxial compression test at different temperatures: (a) 298 K, (b) 1273 K, and (c) 1398 K.



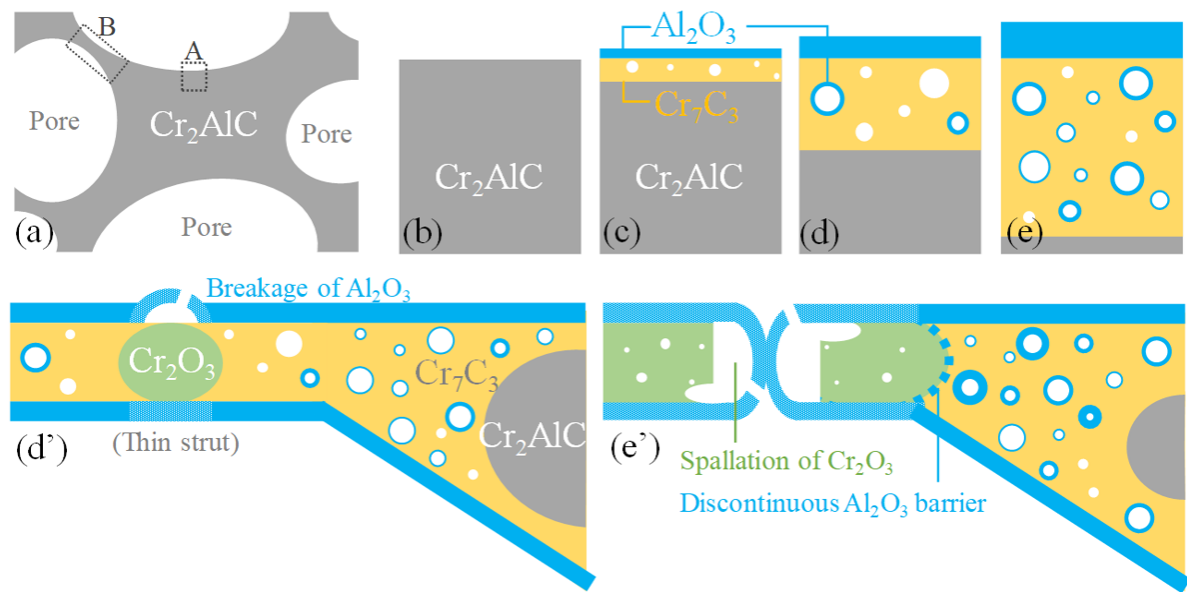
**Figure 4** Compressive strength and  $\text{Al}_2\text{O}_3$  thickness of porous  $\text{Cr}_2\text{AlC}$  annealed at 1473 K for different hours, obtained in the uniaxial compression test at different temperatures: (a) 298 K, (b) 1273 K, and (c) 1398 K. The symbol \* represents the specimen annealed at 1373 K for 1 h. The symbols ○ and ● express predominant mechanical behaviours: ○ is for brittle fracture, whilst ● is for plastic deformation.



**Figure 5** Young's modulus of porous  $\text{Cr}_2\text{AlC}$  annealed at 1473 K for different hours, obtained in the uniaxial compression tests at 298 K with relation to (a)  $\text{Al}_2\text{O}_3$  thickness and (b) compressive strength at 298 K. The symbol \* represents the specimen annealed at 1373 K for 1 h. The inset in (b) shows the strength vs the fracture strain relationship.

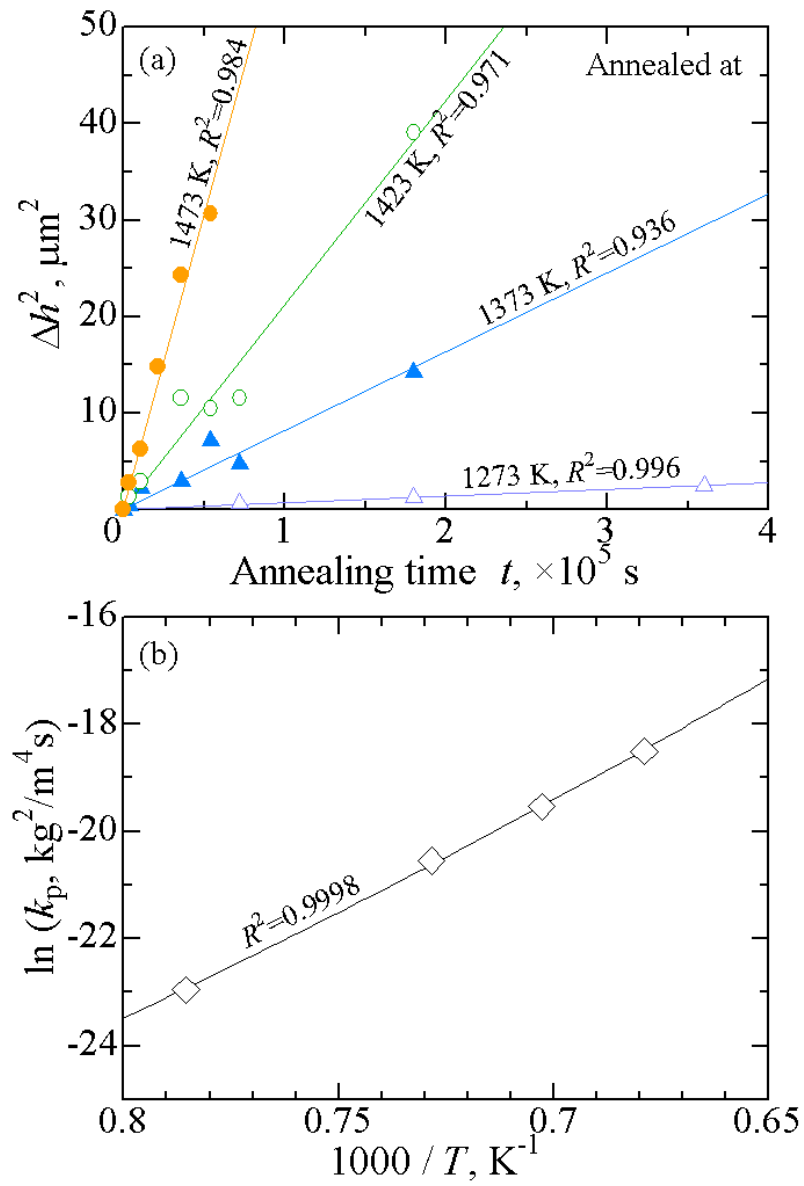


**Figure 6** Fracture surface of porous  $\text{Cr}_2\text{AlC}$  annealed at 1473 K for different hours tested in the uniaxial compression at different temperatures: (a-c) and (d-f) are fractured at 298 K and 1273 K respectively, whilst (a)(d), (b)(e), (c)(f) are annealed for 0, 3, and 20 h, respectively. The white and grey arrows indicate the cracks along grain boundaries and the delaminations in grains, respectively.

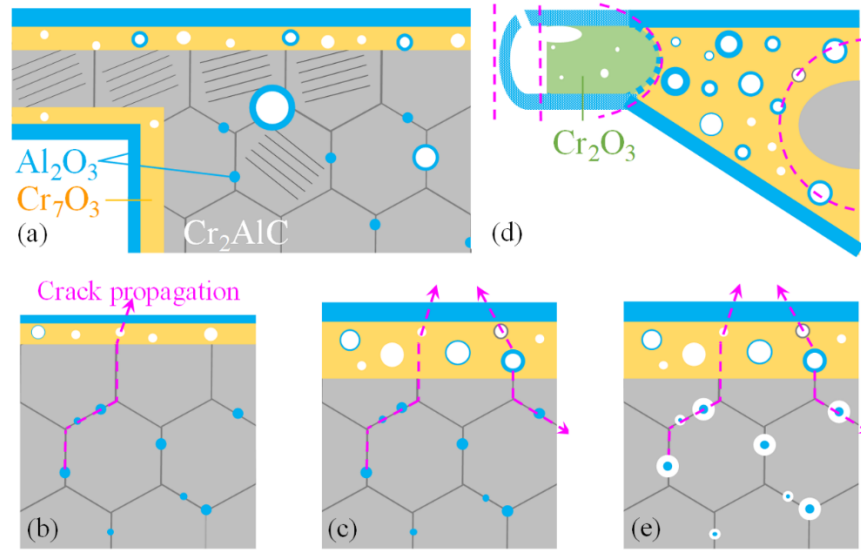


**Figure 7** Oxidation mechanism of porous  $\text{Cr}_2\text{AlC}$ : (a) General view, (b)-(e) oxidation process on the surface of  $\text{Cr}_2\text{AlC}$  (e.g. area A in (a)), and (d')(e') oxidation process around thin strut (e.g. area B in (a), corresponding stage to (d) and (e)).

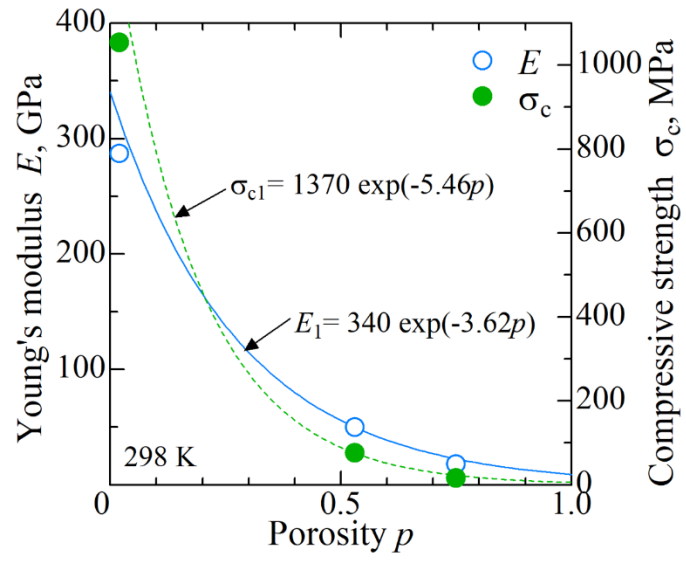




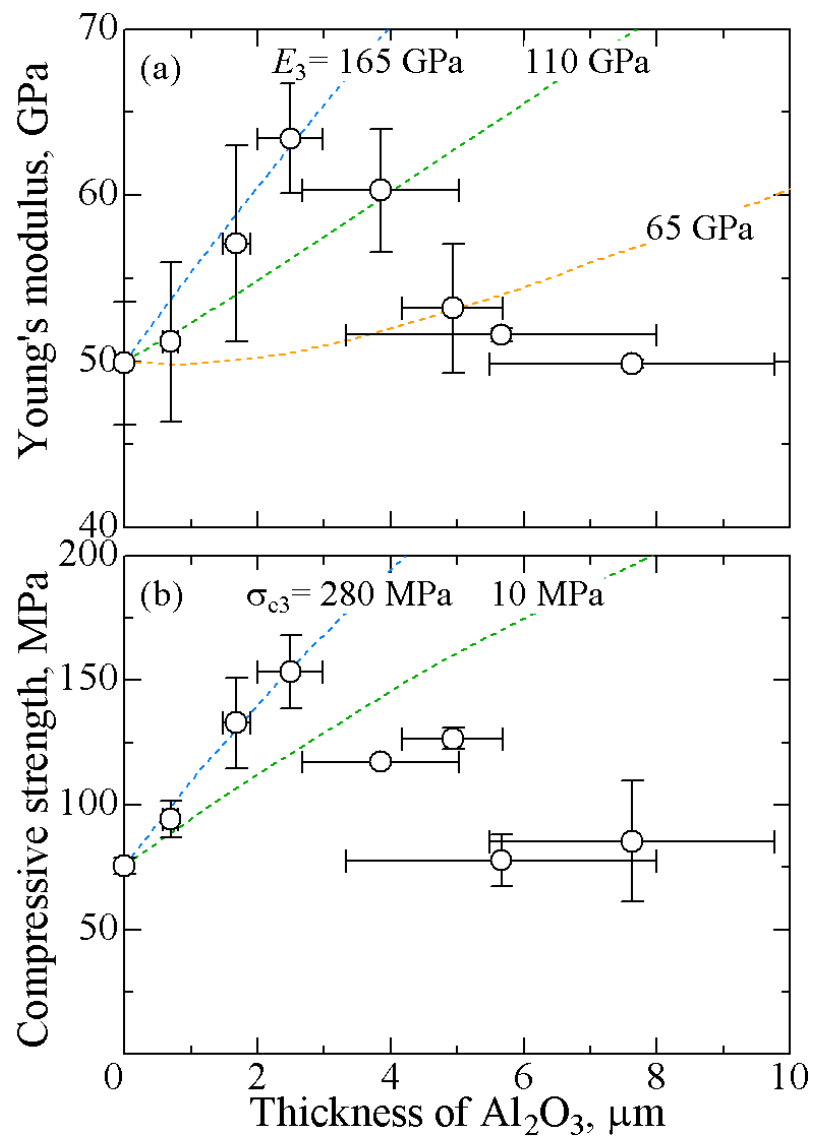
**Figure 8**  $\text{Al}_2\text{O}_3$  growth on porous  $\text{Cr}_2\text{AlC}$  oxidised under different conditions: (a) Approximations by the parabolic law and (b) Arrhenius plot of oxidation constant.



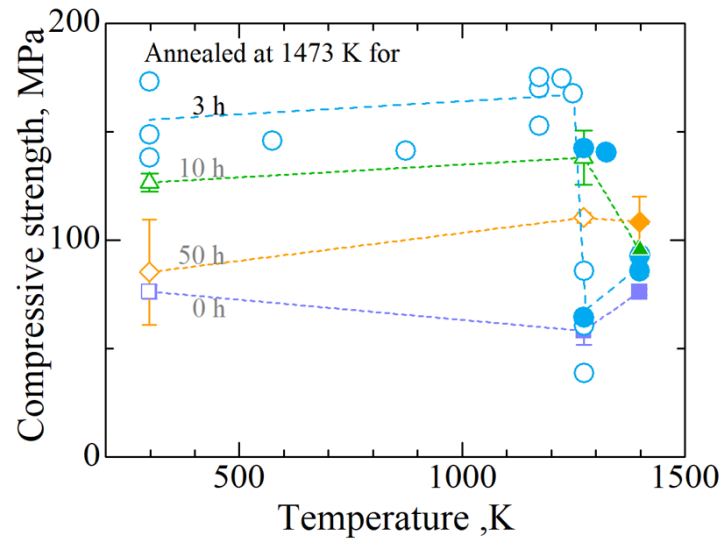
**Figure 9** Fracture mode with crack propagation path in oxidised porous  $\text{Cr}_2\text{AlC}$ : (a)  $\text{Al}_2\text{O}_3$  particles at the grain boundaries and transgranular fractures with delaminations (shown as striped patterns) in the constrained grains, (b) intergranular fracture in a slightly-oxidised sample, (c) in a more oxidised sample, (d) in an excessively-oxidised sample (corresponding to Fig. 7(e')), and (e) intergranular fracture with dimple formations at high temperatures. The dashed lines indicate possible crack propagation paths.



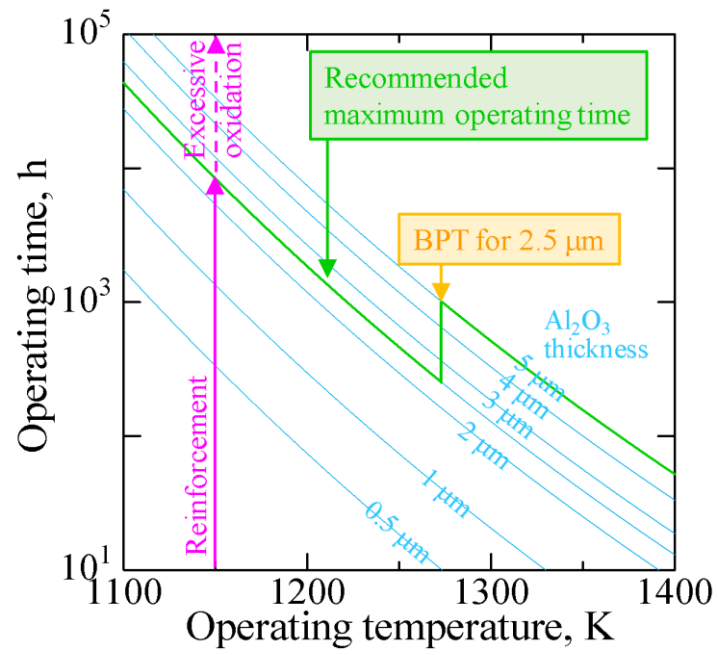
**Figure 10** Mechanical properties of Cr<sub>2</sub>AlC with different porosities obtained in the uniaxial compression test at 298 K and the approximations.



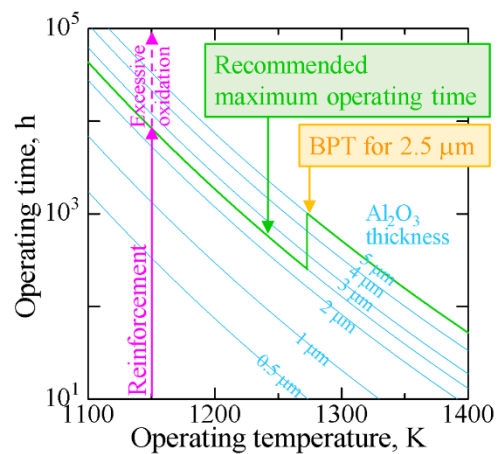
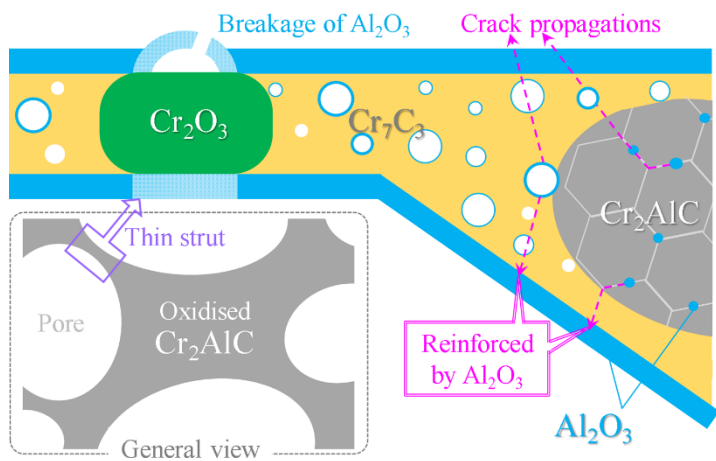
**Figure 11** Predictions of mechanical properties of oxidised porous Cr<sub>2</sub>AlC at 298 K: (a) Young's modulus and (b) compressive strength.



**Figure 12** Compressive strength of porous  $\text{Cr}_2\text{AlC}$  annealed at 1473 K for 3 h as a function of temperature from 298 K to 1398 K. The strength of porous  $\text{Cr}_2\text{AlC}$  annealed at 1473 K for 0, 10, and 50 h are shown for comparison. The open and filled symbols represent brittle fracture and plastic deformation, respectively.



**Figure 13** Recommended operating condition with  $\text{Al}_2\text{O}_3$  thickness. The optimum  $\text{Al}_2\text{O}_3$  thickness is assumed to be  $2.5 \mu\text{m}$  for the temperature  $T \leq 1273 \text{ K}$  and  $5 \mu\text{m}$  for  $T \geq 1273 \text{ K}$ , respectively, whilst the BRT (the brittle-to-plastic transition temperature) is  $1273 \text{ K}$  for the  $\text{Al}_2\text{O}_3$  thickness of  $2.5 \mu\text{m}$ .



**Graphical Abstract**